Portugaliae Electrochimica Acta 2009, 27(3), 381-396

DOI: 10.4152/pea.200903381

PORTUGALIAE ELECTROCHIMICA ACTA
ISSN 1647-1571

Mass Transport and Potential Studies in a Flow-through Porous Electrode Reactor. A Comparative Study of Reticulated Vitreous Carbon and Graphite Felt Used as Cathode

J.L. Nava,[1,*] A. Recéndiz,[1] L.G. González,[2] G. Carreño,[2] F. Martínez[2]

[1] *Universidad Autónoma Metropolitana-Iztapalapa, Departamento de Química, C.P. 09340, México D.F., México*
[2]*Universidad de Guanajuato, Facultad de Ingeniería en Geomática e Hidráulica, Av. Juárez No. 77, CP. 36000, Guanajuato, Guanajuato, México*

Received 25 April 2008; accepted 20 November 2008

Abstract

This paper deals with the use of reticulated vitreous carbon (RVC) and graphite felt (GF) as porous electrode for the removal of 20 ppm Cu(II) in 0.5 mol dm^{-3} Na_2SO_4 at pH 2 (which resembles a rinsing wastewater generated by a plating industry). The experimental mass transport characterization ($k_m a = \mathbf{b}u^{\mathbf{c}}$) showed that for 100 ppi (RVC), the value of the coefficient **b**, associated with magnitude of porous electrode, is 0.88, while for (GF) is 3.38. On the other hand, **c** value for 100 ppi (RVC) is 0.06, while for (GF) is 0.62, indicating that the flow pattern is a complex function of the shape of the electrode. The experimental potential drop for 100 ppi (RVC) and (GF) (1.2 cm thick), indicated the absence of hydrogen evolution. Current efficiencies for RVC and GF were function of convection, giving values comprised between $45 \leq \phi \leq 68\%$ and $51 \leq \phi \leq 73\%$, respectively, and energy consumption values of $0.3 < E_{cons} < 1.7$ and $0.4 < E_c < 1.1$ kWh m^{-3}, respectively. Theoretical number of identical cells in the stack (N) necessary to the cupric depletion from 20 to 1 ppm, for 100 ppi (RVC) and (GF) were calculated.

Keywords: metal ion removal, rinsing wastewater, flow-through porous electrode reactor, mass transport characterization, potential drop.

Introduction

In general the plating industry generates great amounts of aqueous effluents, which contain heavy metals in solution originated from the rinses of coated items. The removal of these metals is traditionally carried out by

* Corresponding author. E-mail address: jlnm@xanum.uam.mx

physicochemical methods where different metals are precipitated as hydroxides, generating great amounts of sludge that should be subsequently confined. Despite this treatment, solubility limits of heavy metals in many instances exceed those allowed by environmental legislation.

Electrochemical technologies have recently attracted attention, for they allow metal recovery in its most valuable form (zero-oxidation state), without requiring addition of chemicals, and thereby not generating byproducts which would later require treatment or confinement [1-4]. Moreover, electro-recovered metals and waters treated using these electrochemical methods can be reused in the same process. This avoids economic loss during treatment, and reduces both water consumption and environmental impact.

Flow-through porous electrodes are usually used for electrochemical recovery of heavy metals from very dilute solutions [5-11]. This electrochemical reactor provides large surface area usually depleting the concentration of metal ions below 0.1 ppm.

Several forms of flow-through porous electrodes have been employed for the removal of heavy metals, such as graphite felt (GF) [12], carbon particles [5], zinc spheres [9], silver coated glass [13], platinum screen [14], reticulated vitreous carbon (RVC) [8, 15], stainless-steel fibers [16], nickel felts and nickel foams [17], to mention some of them. Experimental mass transport correlations obtained in this kind of flow-through reactors, when electrodes usually work under mass transport control, evidenced disagreement between authors. This last is attributed to the electrode material, shape, electrode area, and reaction mechanism (nature of the new metallic phase) involved.

On the other hand, it is well known that during the depletion of the metal ions from the solutions, a potential and current distribution along the cathode occurs [5-10]. For this reason, it is highly recommendable to design thick porous electrodes with moderate flow rate of electrolyte [5-6] to avoid secondary reactions which impact in the performance of the flow through porous electrode.

This paper deals with the use of reticulated vitreous carbon (RVC) and graphite felt (GF) as porous electrode for the removal of 20 ppm Cu(II) in 0.5 mol dm^{-3} Na_2SO_4 at pH 2 (which resembles a rinsing wastewater generated by a plating industry). Experimental mass transport and potential drop characterization in both electrode materials were obtained. Theoretical number of cells in the stack (N) necessary to the cupric depletion from 20 to 1 ppm as a function of hydrodynamics, for RVC and GF were calculated.

This paper shows a methodology for the design of thick porous electrode(s) to be used for the removal of metal ions from very dilute concentrations, with moderate flow rate of electrolyte, avoiding hydrogen evolution reaction. This has an impact on the current efficiency and energy consumption during the electrolysis process.

Mass balance in the flow-through porous electrode reactor

The concentration profile of the electroactive species along a porous electrode, under mass transport control, in a continuous single pass reactor, not considering

phase changes and dispersion effects, can be described by the following equation [16, 18]:

$$C(z) = C(z=0)\exp\left[-\frac{k_m a(1-\varepsilon)}{u} z\right] \quad (1)$$

where C(z=0) and C(z) are the concentrations of the electroactive species at the inlet of the packed electrode in z = 0 and at the z point along the electrode length, respectively (Fig. 1). k_m is the average mass transport coefficient assuming that it is independent of axial position, a is the volumetric surface electrode area (a=electrode area/volume occupied by the whole electrode), ε is the electrode porosity, and u is the mean linear electrolyte velocity in an empty channel of the same dimensions.

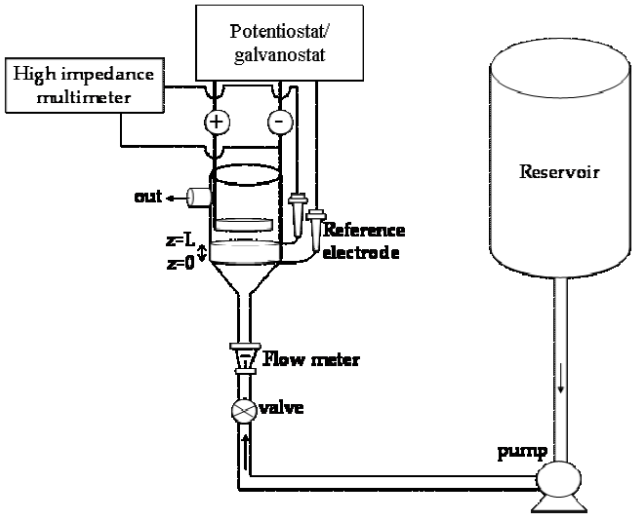

Figure 1. Electrical and flow circuit for the measurement of electrochemical removal of cupric ions at flow-through porous electrode reactor.

When designing a flow-through porous electrode reactor, it is necessary to know the mass transfer rate towards the electrode surface in given hydrodynamic conditions. The mass transport correlations in flow-through porous electrodes can be expressed as equation (2):

$$k_m a = \mathbf{b} u^{\mathbf{c}} \quad (2)$$

where **b** is a constant associated with shape and cell dimensions, and **c** is a constant associated with hydrodynamics. The mass transport correlation is best evaluated through analysis of experimental data, and it varies with respect to the electrode material and reaction mechanism (nature of the new metallic phase) involved on the flow-through porous electrode [14].

Experimental

The solution employed for the electrochemical tests consists of 3.1×10^{-4} mol dm^{-3} (20 ppm) Cu(II), 0.5 mol dm^{-3} Na_2SO_4 at pH 2, prepared using analytical grade reactants dissolved in deionized water (Milli-Q^{TM}).

Equipment

Experiments at the rotating disc electrode (RDE)

A three electrode glass electrochemical cell of 100 milliliters (mL) capacity with a nitrogen inlet was used. The working electrodes were two disks, the first of vitreous carbon, and the second of graphite, both of them with area of A = 0.079 cm^{-2}; the electrode surface was polished with wet 0.3 micrometers (μm) alumina powder and rinsed with distilled water followed by 5 minutes of ultrasonic bath, and a final rinse with distilled water was made before each experiment. The ultrasonic bath removes the traces of alumina left on the electrode surface. When following this method of pre-treatment, the test results were perfectly replicable. The experiments were made at 25 $\pm$ 3 °C under nitrogen atmosphere. The reference and counter electrodes were $Hg/Hg_2SO_4(s)/K_2SO_4(sat)$ (SSE), Tacussel™ model XR200, immersed into a Luggin capillary, and a graphite bar, respectively. A Tacussel™ rotating disk electrode assembly model F69100, a CTV-101 Radiometer Analytical™ and a potentiostat-galvanostat PAR™ Model 273A were used. All potentials shown in this article were corrected and reported against the standard hydrogen electrode (SHE).

Experiments in the flow-through porous electrode reactor

Fig. 1 shows a schematic diagram of the flow cell; the body of the reactor consists of a glass tube of 7.2 cm of inner diameter and 8.5 cm length, with a conical shape at the inlet and a tube attached to the body of the cell as the exit.

The glass tube contained RVC and GF as cathode electrode. A stainless steel cathodic ring collector of 7.2 cm diameter, 1.5 cm wide and 0.3 cm thick was recessed into the body of the cell. The cathode materials (6.5 cm diameter × 1.2 cm thick) were fitted tightly into the cathodic collector; the electrical contact with the current collector was made by gluing RVC and GF electrodes to the current collector with conducting carbon cement (Leit-C from Agar Aids). Table 1 shows the parameters of cathode materials and cell dimensions.

Table 1. Electrode dimensions.

Volumetric area (RVC), a	66 cm^{-1}
Volumetric area (GF), a	517 cm^{-1}
Overall voidage (RVC), ε	0.97
Overall voidage (GF), ε	0.97
Cross sectional area of electrodes, S	31.8 cm^2
Electrode thickness, L	1.2 cm

a and ε were provided by suppliers.

The 100 pores per inch (ppi) RVC and GF were purchased from Electrosynthesis Co.; a titanium mesh covered with a layer of RuO_2 was used as counter electrode at the top of the reactor (Fig. 1). Two small plastic tubes inserted on a 3 millimeter (mm) hole drilled on the glass tube were used as Luggin capillaries to

monitor the local electrode potential at the entrance $\varphi(z = 0)$ and at the exit of the packed bed electrode $\varphi(z = L)$ (see Fig. 1).
A March MFG pump of 1/25 horse power (hp) was used to circulate the electrolyte through the reactor and the flow rates were measured using a variable area polycarbonate flow meter (Cole Palmer model F44376LH-8). The electrolyte flow circuit (Fig. 1) was constructed with Master Flex tubing, (C-Flex 6424-16, 0.5 inch diameter). All the valves and three way connectors were assembled with PVC materials. The electrolyte was held in a 5 liter reservoir.
During electrolysis, the concentration of copper ions was determined by Flame Atomic Absorption Spectrometry (220FS SpectraAA Varian Atomic Absorption Spectrometer).
The potential of the electrolyte at the exit of the porous electrode was monitored with a saturated sulphate reference electrode SSE (E = 615 mV *vs*. SHE (standard hydrogen reference electrode)), inserted into Luggin capillary and connected to high impedance multimeter (Agilent 34401A).

Methodology

RDE was tested to determine the potential range in which the Cu(II)/Cu process is controlled by mass transport. On the other hand, mass transport was characterized at the flow-through porous electrode reactor by electrolysis using the two different cathodic materials at different Reynolds numbers.

Determination of electrolysis potential for Cu(II)/Cu(0) reduction process

A series of potential pulses was applied to the RDE, using the cell described in the section *Experiments at the rotating disc electrode (RDE)*, starting from open circuit potential OCP (0.4 *vs.* SHE) in the potential range of $-0.30 \leq E \leq 0.4$ V *vs.* SHE during 10 sec, with increments of 0.05 V. The corresponding chronoamperograms were obtained at $\omega = 31.2$ s^{-1}. From these chronoamperograms, sampled current density (at 5 seconds) *vs*. cathodic potential pulse curves were constructed (J-E). It is important to point out that the copper process on the vitreous carbon and graphite disks was assumed to have the same electrochemical response as that obtained on the 100 ppi RVC and carbon felt, respectively [19]. On the other hand, the authors decided to construct the polarization curves using sampled current density *vs*. cathodic potential instead of linear sweep voltammetry technique, because a voltammetric study always involves the relationship between the formation rate of deposits at the interface and the polarization rate of the electrode. This last problem is eliminated in the potential pulse technique [16, 20].

Experimental evaluation of mass transport coefficients in the flow-through porous electrode reactor in a single pass mode of operation

The experimental determination of $k_m a$ was obtained by the depletion of the concentration of Cu(II) at (z = L), and by means of equation (1), during the electrolysis experiments at holding potential, in the flow through porous

electrode reactor in a single pass mode of operation. These experiments were performed in the potential range with a limiting current plateau, which guaranteed the mass transport control of the process.
The electrolysis potential was -0.1 V *vs.* SHE imposed at the entrance of the reactor (z = 0) (see Fig. 1); this value was taken from RDE tests. The studies were performed at linear flow velocities comprised between $0.05 \leq u \leq 0.25$ cm s^{-1}. This set of electrolysis conditions was applied to RVC and GF. Concentration of cupric ions was determined by Flame Atomic Absorption Spectroscopy Analysis (FAAS). It is important to point out that each concentration result required around 5 minutes of stable operation of the reactor.

Experimental evaluation of the potential drop during the Cu(II)/Cu process in the flow-through porous electrode reactor
The electrode potential at the exit (z=L) of the flow-through porous electrode was monitored with a saturated sulphate reference electrode SSE (E = 615 mV *vs*. SHE) (see Fig. 1). The potential drop was estimated by the difference between the electrode potential at the exit and inlet ($\Delta\varphi = \varphi(z=L) - \varphi(z=0)$). These analyses lead to confirm the absence of parasitic reactions, such as hydrogen evolution, during the Cu(II)/Cu process on RVC and graphite felt. It is important to point out that each result in electrode potential required around 5 minutes of stable operation of the reactor.

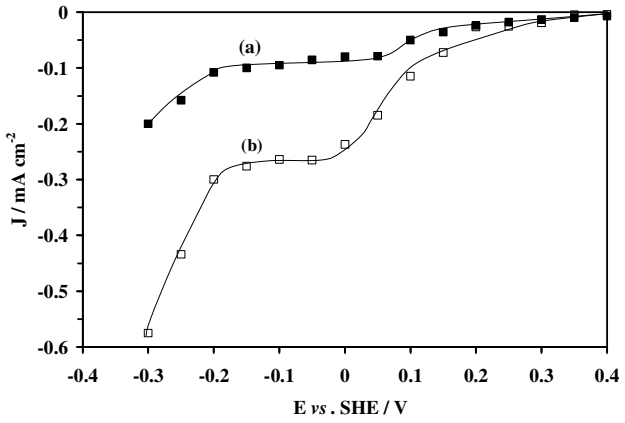

Figure 2. Typical sampled current density *vs*. cathodic potential curves for Cu(II) ions deposition process, constructed from typical current density transients at sampling time of 5 s, at angular velocity of 31.2 s^{-1}. RDE of: (a) vitreous carbon and (b) carbon. Electrolyte: 3.1×10^{-4} mol dm^{-3} (20 ppm) Cu(II), 0.5 mol dm^{-3} Na_2SO_4 at pH 2. This composition resembles a rinsing wastewater generated by a plating industry. A = 0.079 cm^{-2}. It is important to mention that the lines that connect points only make data reading easier without indicating a linear fit.

Analysis of results and discussion

Determination of electrolysis potential for Cu(II)/Cu process

Fig. 2 shows typical current density *vs.* cathodic potential curves for Cu(II)/Cu process, constructed from typical current transients at sampling time of 5 s, at ω

= 31.2 s^{-1} on vitreous carbon (a) and graphite (b) disks. Fig. 2(a) present a limiting current plateau, where the process is limited by mass transport, comprised between -0.2 ≤ E ≤ 0.05 V *vs*. SHE; while hydrogen evolution started at E < - 0.2 V *vs*. SHE. In Fig. 2(b) the Cu(II)/Cu process, limited by mass transport, was detected within the potential range of -0.2 ≤ E ≤ 0.0 V *vs*. SHE, and at E < - 0.2 V *vs*. SHE, the hydrogen evolution start to be detected.
The fact that the obtained current on graphite disk (Fig. 2(b)) was higher than that obtained on vitreous carbon disk (Fig. 2(a)), indicates that the former electrode provides more electro-active area; even with both electrodes have the same geometrical area (0.079 cm^2). This last is due to the roughness produced at the end of the polishing procedure.
Considering that 100 ppi RVC and GF have the same electrochemical responses to those vitreous carbon and graphite disks, respectively, the limiting current plateau for RVC and GF are comprised between (-0.2 ≤ E ≤ 0.05 V *vs*. SHE) and (-0.2 ≤ E ≤ 0.0 V *vs*. SHE), respectively.

Mass transport and potential drop characterization in the flow-through porous electrode during the Cu(II)/Cu process

For the electrolysis experiments in the flow-through porous electrode reactor (Fig. 1), with RVC, a potential of $\varphi(z=0)$ = - 0.1 V *vs*. SHE, was applied at the entrance of the electrode in order to ensure that the electrolysis occurs under mass transport control. It is important to mention that the depletion of the concentration of Cu(II), along the axis of the electrode, gives a potential distribution, hence it is necessary to control that at the exit (z=L), the potential does not exceed more negative values than $\varphi(z=L)$ < - 0.2 V *vs*. SHE, with the aim to avoid hydrogen evolution reaction. For the above, the maximum potential drop on RVC is $\Delta\varphi = \varphi(z=L)-\varphi(z=0)$ = - 0.2 – (-0.1) = - 0.1 V. On the other hand, the maximum potential drop for GF will be: $\Delta\varphi = \varphi(z=L)-\varphi(z=0)$ = - 0.2 – (-0.1) = - 0.1 V. It is important to point out that such criterion for the estimation of the maximum potential drop was previously proposed by Kreysa et al. [21] and Nava et al. [16]. The mean linear flow velocities, u, during the electrolysis, were between 0.05 and 0.25 cm s^{-1}. Fig. 3 shows the normalized copper concentration ($C_{Cu(II)}(z=L)$ / $C_{Cu(II)}(z=0)$) *vs.* mean linear flow electrolyte velocity (u) in a flow-through reactor with 3D: (a) RVC and (b) GF electrodes.
From the analyses of Fig. 3 (a) and (b) it is observed that normalized cupric concentration increases as a function of linear flow velocity, which is in agreement to that described by equation (1) and previously reported by other authors [8]. On the other hand, the depletion of normalized copper concentration on GF was more quantitative to that obtained on RVC, at 0.1 ≤ u ≤ 0.25 cm s^{-1}, due to the fact that GF has greater volumetric area (517 cm^{-1}) than RVC (66 cm^{-1}). It is important to point out that at linear flow velocity of 0.05 cm s^{-1}, this ratio trends to invert, which can be associated to a change in the flow pattern inside RVC.

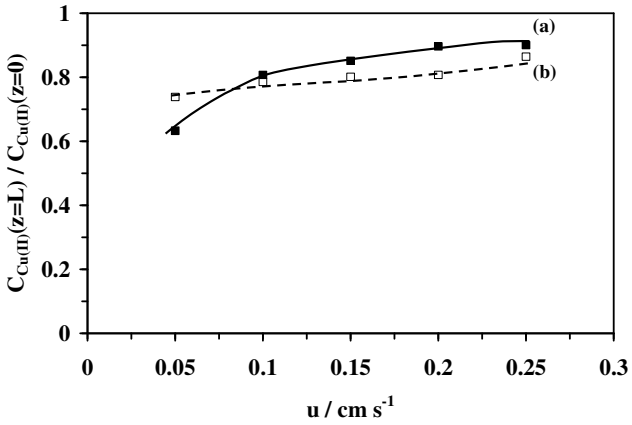

Figure 3. Normalized copper concentration *vs.* mean linear flow electrolyte velocity in a flow-through reactor with 3D: (a) 100 ppi RVC and (b) carbon felt electrode. Electrolyte: 3.1 × 10^{-4} mol dm^{-3} (20 ppm) Cu(II), 0.5 mol dm^{-3} Na_2SO_4 at pH 2. This composition resembles a rinsing wastewater generated by a plating industry. All the electrolyses were performed at holding potential of φ (z = 0) = −0.1 V *vs*. SHE.

Fig. 4 shows the curves $k_m a$, *vs*. u, for RVC and GF electrodes. These values were obtained from the normalized cupric concentration *vs*. mean linear flow velocity (Fig. 3 (a) - (b)), and by applying the equation (1). From the analysis of Fig. 4 the average mass transport coefficients for GF increased with the mean linear flow velocity, due to Nernst diffusion layer is compacted with convection, while for RVC average mass transport coefficients increase slightly with convection. It is important to point out that the values of $K_m a$ presented herein are similar, in order of magnitude, to that obtained by Bertazzoli et al. [15], 0.141, 0.192, 0.223 s^{-1}, for linear flow velocities of 0.22, 0.44 and 0.88 cm s^{-1}, respectively, during the deposit of lead on 80 ppi RVC in a flow-through reactor. However, Bertazzoli et al. did not present a correlation of the type $k_m a = \mathbf{b}u^{\mathbf{c}}$.

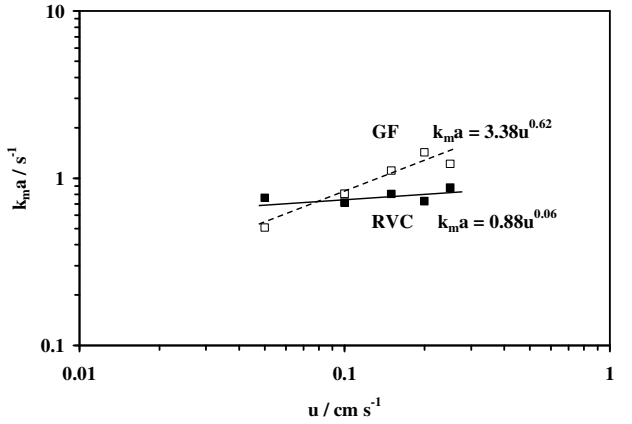

Figure 4. Mass transport coefficients *vs*. mean linear flow electrolyte velocity in a flow-through reactor with 3D: 100 ppi RVC and GF electrode. The mass transport coefficients were evaluated during Cu(II)/Cu process (similar to Fig. 3) and by using equation 1.

From the correlations $k_m a = \mathbf{b}u^{\mathbf{c}}$ showed in Fig. 4, it can be observed that for RVC, the value of the coefficient **b** is 0.88, while for GF is 3.38, as was expected, since constant **b** is associated with the volumetric surface area and shape of porous electrode [22]. On the other hand, the values of the exponent **c** for RVC are 0.06, while for GF is 0.62, indicating that the flow pattern is a complex function of the specific surface area, electrode porosity and shape of the electrode [12, 16].
In Table II, the mass transport correlation for GF, obtained in this work, is compared to that reported in the literature. It is important to point out that the correlations obtained by Delanghe et al. [12] were obtained in two electrolytic solutions, with an electrode thickness of 0.9 cm, the former during the deposition of mercury, and the latter during the soluble reduction of $Fe(CN)_6^{3+}$/ $Fe(CN)_6^{2+}$. From the analysis of these two correlations and the obtained herein, it is clearly observed that the nature of reduction reaction and the volumetric surface area modify the mass transport correlation [12].

Table 2. Mass transfer correlations in flow-through porous electrode.

Electrolytic solution	$k_m a = bu^c$	
	GF	RVC
Cu^{2+}	$3.38u^{0.62}$ (this work)	$0.88u^{0.06}$ (this work)
Hg^{2+}	$3.7u^{0.42}$ [12]	——
$Fe(CN)_6^{3-}$	$6.0u^{0.36}$ [12]	——
—	——	$0.002u^{0.08}$ (60 ppi) [23]

On the other hand RVC correlation, obtained herein, is compared to that informed in reference [23] (Table II), showing marked differences in the value of **b**, while the value of the exponent **c** is close in both correlations; such variations may be associated with the difference in pore per inch of RVC, 100 and 60 ppi, this work and obtained in reference [23], respectively. It is important to mention that correlation of the type $k_m a = \mathbf{b}u^{\mathbf{c}}$ for RVC and GF are rather limited in the literature.
The comparison of mass transport correlations supports the well known that in flow-through porous electrode the best correlation is the obtained through experimental data, because it depends on the geometry of the electrode, type of fluid flow pattern, and the reaction mechanism (nature of the new metallic phase) [12].

Fig. 5 shows the experimental potential drop in a flow-through reactor with 3D: (a) RVC and (b) GF, measured during the electrolysis showed in Fig. 3 (a) and (b). From the analysis of Fig. 5(b) it is observed that the potential becomes more negative as mean linear flow velocity increases, while the potential drop remains constant in Fig. 5 (a). The experimental potential drop decay with convection is

in agreement to that reported from the literature [5]. Nevertheless, the potential drop in RVC, Fig. 5(a) is different that the expected, which can be due to the fact that depletion of cupric ions is little significant on RVC, as was shown in Fig.3(a).

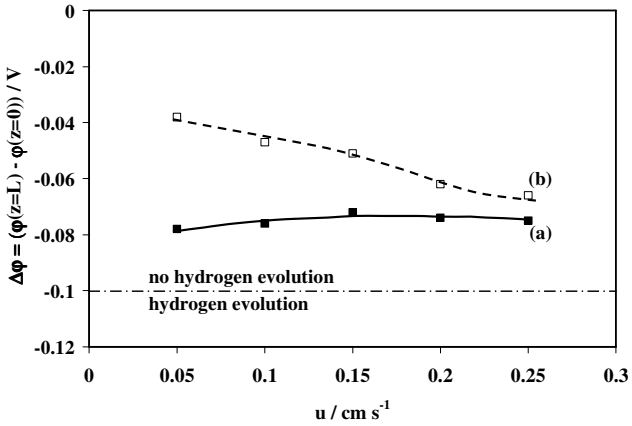

Figure 5. Experimental potential distribution *vs*. mean linear flow electrolyte in a flow-through reactor with 3D: (a) 100 ppi RVC and (b) GF electrode. The potential drop ($\Delta\varphi = \varphi(z=L) - \varphi(z=0)$) was evaluated during Cu(II)/Cu process (similar to Fig. 3).

The potential drop in the flow-through with RVC and GF was fitted with a model provided in literature [16, 24]; however, the experimental data obtained herein were higher, in one magnitude order, than those obtained theoretically. This last can be due to some potential distribution on the electrode matrix of RVC and GF. For the purpose of this paper, the experimental potential drop in the flow-through electrode of RVC and GF, at $0.05 \leq u \leq 0.25$ cm s^{-1} and 1.2 cm thick, indicates the absence of hydrogen evolution.

Fig. 6 shows current efficiencies of the Cu(II)/Cu process at the flow-through reactor with RVC and GF for the electrolyses shown in Fig. 3. These were obtained using equation 3 [23]:

$$\phi = \frac{zF\Delta C_{Cu(II)} V_R}{Q} \times 100 \qquad (3)$$

where $\Delta C_{Cu(II)} = (C_{Cu(II)}(t=0) - C_{Cu(II)}(t))$ in mol dm^{-3}, V_R, is the solution volume in dm^3, and Q is the total charge employed in the electrolysis in coulomb.

The analysis of Fig. 6 demonstrates the dependence of current efficiencies on the mean linear flow velocity; particularly, for RVC (a) current efficiencies increase linearly with convection from 45 to 68%. For GF (b) efficiency increases with convection at velocities comprised between $0.5 \leq u \leq 0.15$ cm s^{-1} ($51 \leq \phi \leq 86$), and for u = 0.20 cm s^{-1} this value increases lowly, $\phi = 87$, then at u = 0.25 cm s^{-1}, current efficiency decreases giving a value of $\phi = 73\%$; these last value can be associated to a change in the flow pattern inside GF, similar to that observed in mass transport studies showed in Fig. 4. The dependence of current efficiencies obtained herein are in contrast to that obtained by El-Deab et al. [7], who showed that current efficiencies decrease with convection, during the deposit of lead ions (40 ppm) in basic media in a flow-through electrode of stacked copper screens.

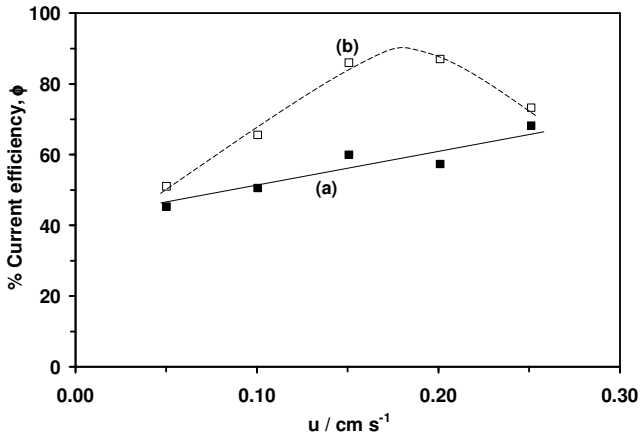

Figure 6. Integral current efficiency *vs*. mean linear flow electrolyte in a flow-through reactor with 3D: (a) 100 ppi RVC and (b) GF electrode. Current efficiencies were evaluated during Cu(II)/Cu process (similar to Fig. 3) and by using equation 3.

The values obtained by El-Deab et al. were between $99 \leq \phi \leq 52\%$ at velocities comprised between $0.93 \leq u \leq 8.6$ cm s^{-1}. The differences in the current efficiency pattern obtained in this paper may be due to moderate flow velocities with regard to that reported by El-Deab et al. [7], which can be associated with the residence time and the interaction between metal ion and porous electrode. On the other hand, the fact that current efficiencies obtained herein were not around 100%, as expected according to potential distribution analysis, which indicates the absence of hydrogen evolution, suggests that some of the current intensity is lost by capacitance phenomena due to the huge electrode area of RVC and GF, and by leakage currents. It is important to mention that experimental current efficiency values are rather limited in the literature for GF and RVC.

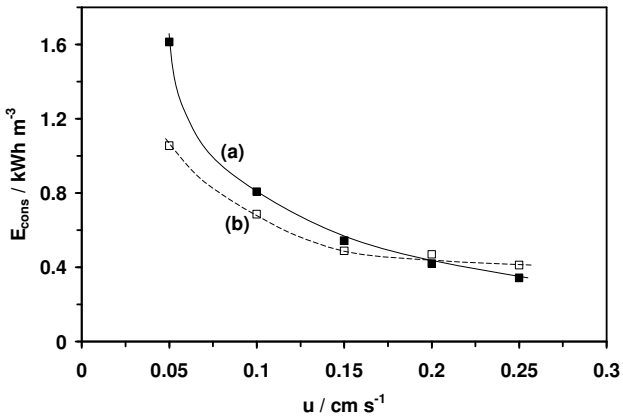

Figure 7. Energy consumption *vs*. mean linear flow electrolyte in a flow-through reactor with 3D: (a) 100 ppi RVC and (b) GF electrode. E_{cons} were evaluated during Cu(II)/Cu process (similar to Fig. 3) and by using equation 4.

Fig. 7 shows energy consumption (E_{cons}) of the Cu(II)/Cu process at the flow-through reactor with RVC (a) and GF (b) for the electrolysis showed in Fig. 3. These were obtained using equation (4) [23]:

$$E_{cons} = \frac{zFE_{cell}\Delta C_{Cu(II)}}{\phi \times 3600} \quad (4)$$

where E_{cell} is the cell potential in volts, and 3600 is a factor that allows obtaining kWh m^{-3} units.

The analysis of Fig. 7 shows that energy consumption decreases with convection for RVC and GF, giving low values for GF between $0.40 < E_{cons} < 1.1$ kWh m^{-3}, at $0.05 \leq u \leq 0.015$ cm s^{-1}; then at $u \geq 0.20$ cm s^{-1} this trend to invert. The E_{cons} values reported in this work are similar to those given in reference [25] which values are between $0.02 < E_{cons} < 0.20$ kWh m^{-3}. The low values of E_{cons} obtained herein for RVC and GF are due to the low concentration of Cu(II) (3.1×10^{-4} mol dm^{-3}) and by the experimental conditions that avoids hydrogen evolution reaction.

From the analysis of Fig. 6 and 7, in connection to that observed in Fig. 4, it can be distinguished that in such 3D electrodes mass transport improvements benefit current efficiency and energy consumption.

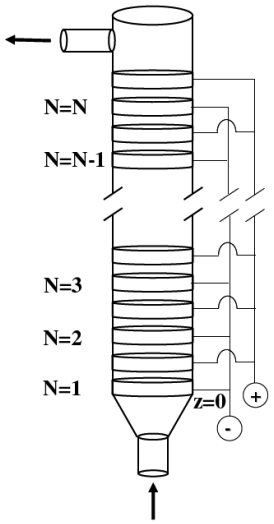

Figure 8. Flow-through porous electrode reactor scheme, including several identical cells in the stack.

It is important to mention that the complete removal of cupric ions, on one single pass at different hydrodynamic conditions, was insufficient (Fig. 3 (a)-(b)). For this last, in an application, it is necessary to design an electrochemical reactor with several cells in the stack (Fig. 8).

Theoretical design of a flow-through porous electrode reactor with several cells in the stack

Fig. 9 (a)-(b) shows number of identical cells in the stack (N) necessary to the cupric depletion from 20 to 1 ppm as a function of hydrodynamics, evaluated by

means of equation (5), for RVC and GF, respectively. This model considers that $k_m a$ does not vary from cell to cell in the stack.

$$C_{Cu(II)}(z = N) = C_{Cu(II)}(z = 0)\exp - \left[\frac{k_m a(1-\varepsilon)L}{u} N \right] \quad (5)$$

From the analysis of Fig. 9(a) for RVC it is observed that number of cells in the stack increases as a function of hydrodynamics; the same behavior is observed in GF (Fig. 9(b)), but less quantitative. It is important to point out that GF requires less number of cells in the stack that RVC, in the interval of $0.1 \leq u \leq 0.25$ cm s^{-1}; while at u of 0.05 this trend is inverted, RVC requires 6 and GF 8 identical cells in the stack. The fact that GF, at u>0.05 cm s^{-1}, requires less number of cells in the stack is due to GF has greater specific area than RVC; while at linear flow velocity of 0.05 cm s^{-1}, this ratio trends to invert.

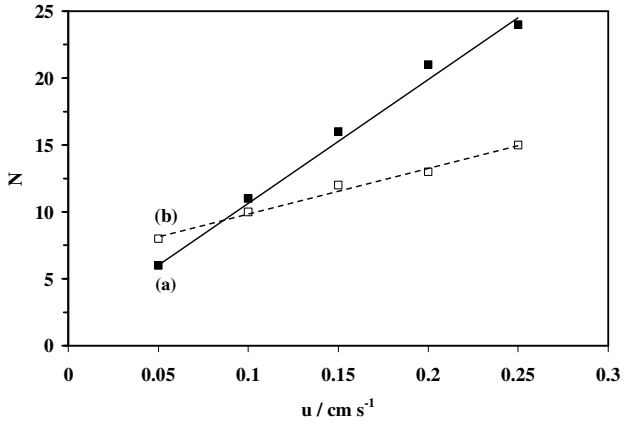

Figure 9. Number of identical cells in the stack *vs*. mean linear flow velocity in a flow-through reactor with 3D: (a) RVC and (b) GF electrode. N was evaluated by means of equation (5), considering cupric depletion from 20 to 1 ppm.

For design purposes, the number of identical cells in the stack predicted by equation (5) can be used as a first approach for the recovery of metals in low concentrations from 20 to 1 ppm, since hydrogen evolution is avoided in the interval of $0.05 \leq u \leq 0.25$ cm s^{-1}, for a fixed thick of 1.2 cm. Experimental validation of this approach may be later validated.

It is important to mention that 3D electrodes need to be replaced periodically due to their plugging during the electrodeposition process, which can be correlated with the pressure drop and Faraday law; however, this analysis may be later incorporated. It is important to remark that in this paper the below mentioned phenomena were omitted due to the low concentration of cupric ions (20 ppm) and the low residence time of electrolysis.

Conclusions

This paper deals with an experimental comparison of using RVC and GF as flow-through porous electrode for removal of cupric ions from acidic dilute solution.

The experimental mass transport characterization ($k_m a = \mathbf{b}u^{\mathbf{c}}$) showed that for RVC, the value of coefficient **b**, associated with magnitude of porous electrode, is 0.88, while for GF is 3.38. On the other hand, the value of the exponent **c** for 100 ppi RVC is 0.06, while for GF is 0.62, indicating that the flow pattern is a complex function of the shape of the electrode.

The experimental potential drop for GF becomes more negative as a function of mean linear flow velocity, from $-0.07 \leq \Delta\varphi \leq -0.04$ V in the interval of $0.05 \leq u \leq 0.25$ cm s^{-1}; while for 100 ppi RVC, $\Delta\varphi$ remains almost constant in a value of -0.08 V. The experimental potential drop in the flow-through electrode made of RVC and GF (1.2 cm thick), indicates the absence of hydrogen evolution.

Current efficiencies for RVC and GF were function of convection giving values comprised between $45 \leq \phi \leq 68\%$ and $51 \leq \phi \leq 73\%$, respectively, and energy consumption values of $0.3 < E_c < 1.7$ and $0.4 < E_c < 1.1$ kWh m^{-3}, respectively.

Theoretical number of identical cells in the stack (N) necessary to the cupric depletion from 20 to 1 ppm as a function of hydrodynamics, for RVC and GF, were calculated. At linear flow velocity of 0.25 cm s^{-1}, six and eight cell stacks are required for RVC and GF, respectively.

List of Symbols

Symbol	Meaning	Units
a	Volumetric surface area of the electrode (electrode area/volume occupied by the whole electrode)	$cm^2\ cm^{-3}$
A	Electrode geometric area	cm^2
b	Constant	
c	Constant	
C(z)	Concentration of electroactive species at any arbitrary position along the axial axes of the packed bed electrode	mol cm^{-3}
C(z=0)	Concentration of electroactive species at the point of z = 0 of the packed bed electrode	mol cm^{-3}
C(z=N)	Concentration at the exit of N-cells in the stack	mol cm^{-3}
E	Potential	V
E_{cell}	Cell potential	V
E_{cons}	Energy consumption	kWh m^{-3}
k_m	Average mass transport coefficient	cm s^{-1}
F	Faraday constant, 96485	C mol^{-1}
J	Current density	A cm^{-2}
L	Electrode thickness, 1.2 cm	cm
n	Number of electrons transferred during electrochemical reaction	
N	Number of identical cells in the stack	
Q	total charge employed in the electrolysis	C
u	Mean linear electrolyte velocity in empty channel	cm s^{-1}
z	Point along the electrode length	cm

Greek symbols

Symbol	Meaning	Units
α	Parameter group, $\frac{k_m a(1-\varepsilon)}{u}$	cm^{-1}
ε	Electrode porosity	Dimensionless
$(1-\varepsilon)$	Fraction occupied by the porous electrode	Dimensionless
φ	Electrode potential	V
$\varphi(z=L)$	Electrode potential at the packed electrode outlet	V
$\varphi(z=0)$	Electrode potential at the packed electrode inlet	V
ϕ	Integral current efficiency	
ω	Angular velocity	s^{-1}

Acknowledgements
Alejandro Recéndiz and Luis G. González are grateful to CONACyT for the obtained grant.

References

1. F.C. Walsh, *Pure Appl. Chem*. 73 (2001) 1819-1837.
2. C.A.R. Ragnini, R.A. Di Iglia, W. Bizzo, R. Bertazzoli, *Water Research* 34 (2000) 3269 3276.
3. C. Ponce de León, D. Pletcher, *Electrochim. Acta* 41 (1996) 533–541.
4. P. Fornari, C. Abbruzzese, *Hydrometallurgy* 52 (1999) 209-222.
5. D.N. Bennion, J. Newman, *J. Appl. Electrochem*. 2 (1972) 113-122.
6. T. Doherty, J.G. Sunderland, E.P.L. Roberts, D.J. Pickett, *Electrochim. Acta* 41 (1996) 519-526.
7. M.S. El-Deab, M.M. Saleh, B.E. El-Anoduli, B.G. Ateya, *J. Electrochem. Soc.* 146 (1999) 208-213.
8. M. Matlosz, J. Newman, *J. Electrochem. Soc.* 133 (1986) 1850-1859.
9. M.M. Saleh, *J. Phys. Chem. B* 108 (2004) 13419-13426.
10. J.M. Trainham, J. Newman, *J. Electrochem. Soc.* 124 (1977) 1528-1540.
11. E.A. Soltan, S.A. Nosier, A.Y. Salem, I.A.S. Mansour, G.H. Sedahmed, *Chem. Eng*. *J*. 91 (2003) 33-44.
12. B. Delanghe, S. Tellier, M. Astruc, *Electrochim. Acta* 35 (1990) 1369-1376.
13. A. Ratel, G. Lacoste, *J. Appl. Electrochem*. 12 (1982) 267-274.
14. R. Alkire, B. Gracon, *J. Electrochem. Soc.* 122 (1975) 1594-1601.
15. R. Bertazzoli, C.A. Rodrígues, E.J. Dallan, M.T. Fukunga, M.R.V. Lanza, R.R. Leme, R.C. Widner, *Braz. J. Chem. Eng*. 15 (1998) doi: 10.1590/S0104-66321998000400008.
16. J.L. Nava, M.T. Oropeza, C. Ponce de León, J. González-García, A.J. Frías-Ferrer, *Hydrometallurgy* 91 (2008) 98-103.
17. J.M. Marracino, F. Coueret, S. Langlois, *Electrochim. Acta* 32 (1987) 1303-1309.
18. T.Z. Fahidy, *Principles of Electrochemical Reactors Analysis*, Elsevier, Amsterdam, 1985.

19. G. Carreño, E. Sosa, I. González, C. Ponce de León, N. Batina, M.T. Oropeza, *Electrochim. Acta* 44 (1999) 2633-2643.
20. F.F. Rivera, J.L. Nava, *Electrochim. Acta* 52 (2007) 5868-5872.
21. G. Kreysa, C. Reynvaan, *J. Appl. Electrochem*. 12 (1982) 241-251.
22. J. M. Friedrich, C. Ponce-de-León, G.W. Reade, F.C. Walsh, *J. Electroanal. Chem*. 561 (2004) 203-217.
23. F.C. Walsh, *A First Course in Electrochemical Engineering,* The Electrochemical Consultancy, Romsey, 1993.
24. R.E. Sioda, *Electrochim. Acta* 16 (1971) 1569-1576.
25. L.H. Mustoe, A.A. Wragg, *J. Appl. Electrochem*. 13 (1983) 507-517.